International Journal of Thermophysics, Vol. 26, No. 5, September 2005 (© 2005)
DOI: 10.1007/s10765-005-8090-9

A Thermodynamic Property Model for the Binary Mixture of Methane and Hydrogen Sulfide

N. Sakoda[1,2] **and M. Uematsu**[1]

Received November 15, 2004

A thermodynamic property model with new mixing rules using the Helmholtz free energy is presented for the binary mixture of methane and hydrogen sulfide based on experimental $P\rho Tx$ data, vapor–liquid equilibrium data, and critical-point properties. The binary mixture of methane and hydrogen sulfide shows vapor–liquid–liquid equilibria and a divergence of the critical curve. The model represents the existing experimental data accurately and describes the complicated behavior of the phase equilibria and the critical curve. The uncertainty in density calculations is estimated to be 2%. The uncertainty in vapor–liquid equilibrium calculations is 0.02 mole fraction in the liquid phase and 0.03 mole fraction in the vapor phase. The model also represents the critical points with an uncertainty of 2% in temperature and 3% in pressure. Graphical and statistical comparisons between experimental data and the available thermodynamic models are discussed.

KEY WORDS: critical curve; equation of state; Helmholtz free energy; hydrogen sulfide; methane; mixtures; thermodynamic properties; vapor–liquid–liquid equilibrium.

1. INTRODUCTION

Natural gas is a multicomponent mixture whose primary component is methane, and its components as well as their compositions vary depending on the source, making it difficult to predict the thermophysical properties of natural gas. The addition of hydrogen sulfide in natural gas gives a change in phase behavior. The critical curve of the binary mixture of methane and hydrogen sulfide is interrupted by the vapor–liquid–liquid

[1] Center for Multiscale Mechanics and Mechanical Systems, Keio University, Hiyoshi 3-14-1, Kohoku-ku, Yokohama 223-8522, Japan.
[2] To whom correspondence should be addressed. E-mail: ud06599@educ.cc.keio.ac.jp

equilibrium (VLLE) at a mixture of near 0.9 mole fraction of methane, with the other branch starting from the critical point of hydrogen sulfide and diverging near 0.5 mole fraction in the high-pressure region. The binary mixture of methane and hydrogen sulfide is classified as Type III according to Scott and van Konynenburg [1], which is explained in detail in the textbook written by Rowlinson and Swinton [2]. In 1951, Reamer et al. [3] were the first to measure $P\rho Tx$, vapor–liquid equilibrium (VLE), and critical-point data of this mixture. Kohn and Kurata [4] measured VLE data over the wide temperature range from 189 to 366 K as well as critical points in 1958. Their experimental results show complicated phase behavior and a critical curve of Type III.

Cubic equations of state can represent complicated phase behavior and divergences of the critical curve. The Peng–Robinson (PR)-type equations of state that were developed by Endo et al. [5] for natural gas systems are well suited for describing the phase behavior and the critical curve of the binary mixture of methane and hydrogen sulfide. However, cubic equations of state are not able to accurately describe density data in the liquid phase. Recently, a number of accurate equations of state for fluids and fluid mixtures have been presented that use the Helmholtz free energy fundamental property. These equations of state can have many parameters and can represent the thermodynamic properties accurately. However, complicated phase equilibria and critical curves have not yet been calculated from these equations of state because of the complexity of the calculation procedure. In 1999, Lemmon and Jacobsen [6] developed a generalized model for fluid mixtures of hydrocarbons using the Helmholtz free energy function, but they did not include the mixture of methane and hydrogen sulfide.

In this study, we developed a thermodynamic property model for the binary mixture of methane and hydrogen sulfide using the Helmholtz free energy function. The model can accurately represent not only the thermodynamic properties but also the VLE and VLLE behavior as well as the divergence of the critical curve.

2. FUNDAMENTAL EQUATION OF STATE FOR MIXTURES

The Helmholtz equation of state used in this work for a binary mixture is given in Eq. (1) using the dimensionless Helmholtz free energy function ϕ_{mix}. ϕ_{mix} is split into two parts: the ideal-gas part ϕ^0_{mix} and the residual part $\phi^{\text{r}}_{\text{mix}}$.

$$\phi_{\text{mix}} = a/RT = \phi^0_{\text{mix}} + \phi^{\text{r}}_{\text{mix}}, \tag{1}$$

where a is the molar Helmholtz free energy of the mixture in $\mathrm{J \cdot mol^{-1}}$, $R = 8.314472\,\mathrm{J \cdot mol^{-1} \cdot K^{-1}}$ [7] is the universal gas constant, and T is the temperature in K. The ideal-gas part of the binary mixture is given in Eq. (2), which was derived from thermodynamic relations.

$$\phi^0_{\mathrm{mix}} = x_1\phi^0_1(\tau^{\mathrm{pure}}_1, \delta^{\mathrm{pure}}_1) + x_2\phi^0_2(\tau^{\mathrm{pure}}_2, \delta^{\mathrm{pure}}_2) + x_1\ln(x_1) + x_2\ln(x_2), \quad (2)$$

where the dimensionless variables $\tau^{\mathrm{pure}}_i = T_{\mathrm{c},i}/T$ and $\delta^{\mathrm{pure}}_i = \rho/\rho_{\mathrm{c},i}$ are reduced by the critical properties of $T_{\mathrm{c},i}$ and $\rho_{\mathrm{c},i}$ for each pure component i. x_i denotes the mole fraction of component i in the mixture. The residual part is usually fixed empirically. The residual part used here is given in Eq. (3).

$$\phi^{\mathrm{r}}_{\mathrm{mix}} = \sum_{i=1}^{2}\sum_{j=1}^{2} x_i x_j \phi^{\mathrm{r}}_{ij}(\tau, \delta) = x_1^2\phi^{\mathrm{r}}_1(\tau, \delta) + x_2^2\phi^{\mathrm{r}}_2(\tau, \delta) + 2x_1x_2\phi^{\mathrm{r}}_{12}(\tau, \delta), \quad (3)$$

where $\phi^{\mathrm{r}}_1 = \phi^{\mathrm{r}}_{11}$, $\phi^{\mathrm{r}}_2 = \phi^{\mathrm{r}}_{22}$, and $\phi^{\mathrm{r}}_{12} = \phi^{\mathrm{r}}_{21}$. The equation for ϕ^{r}_{12} is given in Eq. (4) as the arithmetic mean of the residual parts of the pure components and the function F_{12}. F_{12} is based on experimental data. The dimensionless variables $\tau = T_{\mathrm{c,mix}}/T$ and $\delta = \rho/\rho_{\mathrm{c,mix}}$ are reduced by the pseudo-critical parameters $T_{\mathrm{c,mix}}$ and $\rho_{\mathrm{c,mix}}$ for the mixture. $T_{\mathrm{c,mix}}$ is calculated with Eq. (5), where $T_{\mathrm{c},12}$ is given in Eq. (6) with the adjustable parameter k_{12}. The pseudo-critical molar volume $v_{\mathrm{c,mix}}$ for the mixture is given in Eqs. (7) and (8), where $v_{\mathrm{c},12}$ is given in Eq. (9) with the adjustable parameter ξ_{12}. $v_{\mathrm{c},i}$ denotes the critical molar volume of pure component i. k_{12} and ξ_{12} are based on experimental data.

$$\phi^{\mathrm{r}}_{12}(\tau, \delta) = F_{12}\left[\phi^{\mathrm{r}}_1(\tau, \delta) + \phi^{\mathrm{r}}_2(\tau, \delta)\right]/2, \quad (4)$$

$$T_{\mathrm{c,mix}} = \sum_{i=1}^{2}\sum_{j=1}^{2} x_i x_j T_{\mathrm{c},ij} = x_1^2 T_{\mathrm{c},1} + x_2^2 T_{\mathrm{c},2} + 2x_1x_2T_{\mathrm{c},12}, \quad (5)$$

$$T_{\mathrm{c},12} = k_{12}\left(T_{\mathrm{c},1} + T_{\mathrm{c},2}\right)/2, \quad (6)$$

$$v_{\mathrm{c,mix}} = 1/\rho_{\mathrm{c,mix}}, \quad (7)$$

$$v_{\mathrm{c,mix}} = \sum_{i=1}^{2}\sum_{j=1}^{2} x_i x_j v_{\mathrm{c,ij}} = x_1^2 v_{\mathrm{c},1} + x_2^2 v_{\mathrm{c},2} + 2x_1x_2v_{\mathrm{c},12}, \quad (8)$$

$$v_{\mathrm{c},12} = \xi_{12}\left(v_{\mathrm{c},1}^{1/3} + v_{\mathrm{c},2}^{1/3}\right)^3 \Big/ 8, \quad (9)$$

where $T_{c,1} = T_{c,11}$, $T_{c,2} = T_{c,22}$, $T_{c,12} = T_{c,21}$, $v_{c,1} = v_{c,11}$, $v_{c,2} = v_{c,22}$, and $v_{c,12} = v_{c,21}$.

The complete dimensionless Helmholtz free energy function for a binary mixture can be expressed as

$$\phi_{\text{mix}} = x_1\phi_1^0(\tau_1^{\text{pure}}, \delta_1^{\text{pure}}) + x_2\phi_2^0(\tau_2^{\text{pure}}, \delta_2^{\text{pure}}) + x_1\ln(x_1) + x_2\ln(x_2) + x_1^2\phi_1^{\text{r}}(\tau, \delta) + x_2^2\phi_2^{\text{r}}(\tau, \delta) + 2x_1x_2\phi_{12}^{\text{r}}(\tau, \delta) \tag{10}$$

3. PROPERTY CALCULATIONS

The functions used for calculating pressure P, fugacity f_i of component i, and molar enthalpy h for a mixture from the dimensionless Helmholtz free energy function, Eq. (10), are given in Eqs. (11)–(13).

$$\frac{P}{\rho RT} = 1 + \delta\left(\frac{\partial\phi_{\text{mix}}^{\text{r}}}{\partial\delta}\right)_{\tau,x_1}, \tag{11}$$

$$\frac{f_i}{\rho RT} = x_i \exp\left(\frac{\partial\left(n\phi_{\text{mix}}^{\text{r}}\right)}{\partial n_i}\right)_{T,V,n_{j\neq i}}, \tag{12}$$

$$\frac{h}{RT} = \tau\left(\frac{\partial\phi_{\text{mix}}^{\text{r}}}{\partial\tau}\right)_{\delta,x_1} + \delta\left(\frac{\partial\phi_{\text{mix}}^{\text{r}}}{\partial\delta}\right)_{\tau,x_1} + \sum_{i=1}^{2} x_i\tau_i^{\text{pure}}\left(\frac{\partial\phi_i^0}{\partial\tau_i^{\text{pure}}}\right) + 1, \tag{13}$$

where n_i denotes the mole number of component i, n is the total number of moles, and V is the volume of the mixture.

The phase equilibrium conditions are given in Eqs. (14) and (15) for binary mixtures using the fugacities of the components calculated from Eq. (12).

$$f_1^{\text{L}}(T, P, x) = f_1^{\text{V}}(T, P, y), \tag{14}$$

$$f_2^{\text{L}}(T, P, x) = f_2^{\text{V}}(T, P, y), \tag{15}$$

where the superscripts "L" and "V" denote the liquid phase and the vapor phase. x and y in Eqs. (14) and (15) refer to the mole fraction in the liquid phase and that in the vapor phase, respectively. Calculating the phase equilibrium for the binary mixture of methane and hydrogen sulfide is complicated by the presence of VLLE. Michelsen [8] proposed a phase equilibrium calculation method using the stability analysis based on the Gibbs free energy. Nitta et al. [9] developed an algorithm suitable for the

phase calculation using Michelsen's method. We used these methods and algorithms for the phase equilibrium calculation.

The conditions for the critical points of binary mixtures are given in Eqs. (16) and (17).

$$\left(\frac{\partial^2 g}{\partial x_1^2}\right)_{T,P} = 0, \tag{16}$$

$$\left(\frac{\partial^3 g}{\partial x_1^3}\right)_{T,P} = 0, \tag{17}$$

where g denotes the molar Gibbs free energy for the mixture as a function of temperature, pressure, and composition. Because the Helmholtz free energy model given in Eq. (10) is represented as a function of temperature, density, and composition, the independent variables for Eqs. (16) and (17) were converted to temperature, molar volume or density, and composition, with the results given in Eqs. (18) and (19). However, it is difficult to find the roots of Eqs. (18) and (19); thus, we used the calculation method proposed by Heidemann and Khalil [10] for the critical-point calculation.

$$\left(\frac{\partial^2 g}{\partial x_1^2}\right)_{T,P} = \left(\frac{\partial^2 a}{\partial x_1^2}\right)_{T,v} + \left[\left(\frac{\partial P}{\partial x_1}\right)_{T,v}^2 \Big/ \left(\frac{\partial P}{\partial v}\right)_{T,x_1}\right] = 0 \tag{18}$$

$$\begin{aligned}\left(\frac{\partial^3 g}{\partial x_1^3}\right)_{T,P} = {} & \left(\frac{\partial^3 a}{\partial x_1^3}\right)_{T,v} + \left[3\left(\frac{\partial P}{\partial x_1}\right)_{T,v}\left(\frac{\partial^2 P}{\partial x_1^2}\right)_{T,v} \Big/ \left(\frac{\partial P}{\partial v}\right)_{T,x_1}\right] \\ & - \left[3\left(\frac{\partial P}{\partial x_1}\right)_{T,v}^2 \left(\frac{\partial^2 P}{\partial x_1 \partial v}\right)_{T} \Big/ \left(\frac{\partial P}{\partial v}\right)_{T,x_1}^2\right] \\ & + \left[\left(\frac{\partial P}{\partial x_1}\right)_{T,v}^3 \left(\frac{\partial^2 P}{\partial v^2}\right)_{T,x_1} \Big/ \left(\frac{\partial P}{\partial v}\right)_{T,x_1}^3\right] = 0\end{aligned} \tag{19}$$

The excess enthalpy h^{E} for binary mixtures at a given temperature, pressure, and composition is calculated with Eq. (20).

$$h^{\mathrm{E}} = h - (x_1 h_1 + x_2 h_2), \tag{20}$$

where h denotes molar enthalpy for the mixture and h_i that for pure component i at the same condition of temperature and pressure for the mixture.

4. AVAILABLE EXPERIMENTAL DATA

We compiled about 1900 experimental thermodynamic property measurements for the binary mixture of methane and hydrogen sulfide. These data are summarized in Table I. Most of the experimental thermodynamic property data are $P\rho Tx$ and VLE data; experimental data for the derived thermodynamic properties are few. In 1951, Reamer et al. [3] first measured $P\rho Tx$, VLE, and critical-point data for the binary mixture of methane and hydrogen sulfide. They reported 1127 points of $P\rho Tx$ data, 76 points of (T, P, ρ^{L}, ρ^{V}, x, y) VLE data, and nine points of critical-point data. These $P\rho Tx$ data cover the temperature range from 278 to 444 K at pressures from 1.4 to 69 MPa in the composition range from 0.1 to 0.9 mole fraction of methane. They reported VLE properties at three temperatures of 278, 311, and 344 K with the critical-point data of these isotherms. In addition, they measured six critical points in the composition range from 0.1 to 0.6 mole fraction of methane.

Bailey et al. [11] in 1987 measured 65 points of $P\rho Tx$ data in the temperature range from 299 to 501 K at pressures up to 38 MPa at a composition of 0.5073 mole fraction of methane. In 1958, Kohn and Kurata [4] measured VLE data over the wide temperature range from 189 to 366 K. However, most of the data are only given in the figures. Only 59 points of (T, P, x, y) VLE data were reported numerically. Phase equilibrium above 278 K, as observed by Reamer et al. [3], shows common VLE behavior. Kohn and Kurata [4] observed VLLE at comparatively low temperatures near 190 K and also the divergence of the critical curve, but they are only shown graphically. In 1959, Kohn and Kurata [13] reported 35 points of (T, P, ρ^{L}, x) and (T, P, ρ^{V}, y) VLE data in the temperature range from 192 to 353 K. Reamer et al. [3] reported the critical-point data at the compositions of 0.55 and 0.6 mole fraction of methane. However, these critical-point data could not be found from the observations of Kohn and Kurata [13]. The critical-point data of Reamer et al. [3] were obtained by extrapolation of dew-point and bubble-point data.

In 1957, Robinson and Bailey [12] measured VLE data for the ternary mixture of methane, carbon dioxide, and hydrogen sulfide at 311 K. In addition, they reported 3 points of (T, P, x, y) VLE data. Robinson et al. [14] measured VLE data for the same ternary mixture at 278 and 344 K in 1959 and reported 5 points of (T, P, x, y) VLE data. These three temperatures of 278, 311, and 344 K are the same as those reported by Reamer et al. [3]. In 1991, Yarym-Agaev et al. [15] reported 124 points of (T, P, x) and (T, P, y) VLE data and 7 points for the critical point. They did not measure the critical-point data directly; these data were determined by extrapolation of VLE data under the premise that the

Table I. Sources of Experimental Thermodynamic Property Data for the Binary Mixture of Methane and Hydrogen Sulfide

				P		ρ		T		x	
Reference[a]	Property[b]	Year	No. of Data	Range (MPa)	δP (kPa)	Range ($\text{mol}\cdot\text{dm}^{-3}$)	$\delta\rho$ ($\text{mol}\cdot\text{dm}^{-3}$)	Range (K)	δT (mK)	Range (mole fraction)	δx (mole fraction)
Reamer et al.* [3]	$P\rho Tx$	1951	1127	1.4–69	0.05%	0.37–26	0.1%	278–444	11	0.10–0.90	0.003
Bailey et al. [11]	$P\rho Tx$	1987	65	0.21–38	0.1%	0.05–9.2	1%	299–501	10	0.5073	0.01%
Reamer et al.* [3]	VLE, y	1951	76	1.2–13	n.a.			278–344	n.a.	0.00–0.73	0.003
Reamer et al.* [3]	VLE, x	1951	76	1.2–13	n.a.			278–344	n.a.	0.00–0.70	0.003
Robinson and Bailey [12]	VLE, y	1957	3	4.1–12	20	–	–	311	56	0.29–0.51	n.a.
Robinson and Bailey [12]	VLE, x	1957	3	4.1–12	20	–	–	311	56	0.03–0.26	n.a.
Kohn and Kurata* [4]	VLE, y	1958	61	1.4–12	14	–	–	189–366	56	0.01–0.97	0.005
Kohn and Kurata* [4]	VLE, x	1958	59	1.4–12	14	–	–	189–366	56	0.00–0.24	0.005
Kohn and Kurata [13]	VLE, y	1959	26	0.05–7.5	14			192–353	n.a.	0.07–0.89	0.005
Kohn and Kurata [13]	VLE, x	1959	9	3.6–12	14			231–353	n.a.	0.07–0.23	0.005
Robinson et al. [14]	VLE, y	1959	5	2.8–11	n.a.	–	–	278–344	110	0.16–0.72	n.a.
Robinson et al. [14]	VLE, x	1959	5	2.8–11	n.a.	–	–	278–344	110	0.02–0.26	n.a.
Yarym-Agaev et al. [15]	VLE, y	1991	78	0.16–13	0.6%	–	–	222–273	n.a.	0.00–0.90	0.002
Yarym-Agaev et al. [15]	VLE, x	1991	46	0.16–12	0.6%	–	–	222–273	n.a.	0.00–0.36	0.002
Reamer et al. [3]	VLE, ρ^{V}	1951	76	1.2–13	n.a.	0.59–15	0.3%	278–344	n.a.	0.00–0.73	0.003
Reamer et al. [3]	VLE, ρ^{L}	1951	76	1.2–13	n.a.	9.0–24	0.3%	278–344	n.a.	0.00–0.70	0.003
Kohn and Kurata [13]	VLE, ρ^{V}	1959	26	0.05–7.5	14	10.03–4.3	3%	192–353	n.a.	0.07–0.89	0.005
Kohn and Kurata [13]	VLE, ρ^{L}	1959	9	3.6–12	14	13–26	3%	231–353	n.a.	0.07–0.23	0.005
Reamer et al.* [3]	C. P.	1951	9	10–13	172	12–15	n.a.	267–361	1.1 K	0.10–0.60	n.a.
Kohn and Kurata [4]	C. P.	1958	2	10–12	14	–	–	337–364	56	0.77–0.93	0.005
Yarym-Agaev et al. [15]	C. P.	1991	7	10–14	0.6%	–	–	229–349	n.a.	0.20–0.80	0.002
Barry et al. [16]	h^{E}	1982	39	0.5–1.5	n.a.	–	–	293–313	n.a.	0.18–0.85	n.a.

[a] Data used as input data are denoted by *.

[b] "VLE, y" and "VLE, x" denote composition data of VLE, where y is the mole fraction of methane in the vapor phase and x is that in the liquid phase. "VLE, ρ^{V}" and "VLE, ρ^{L}" denote saturated density data of VLE, where ρ^{V} is the vapor density and ρ^{L} is the liquid density. "C. P." denotes critical-point data.

critical curve of the binary mixture of methane and hydrogen sulfide is continuous. The distribution of $P\rho Tx$ data is shown in Fig. 1. The distribution of VLE data and that of saturated density data are shown in Fig. 2 on the P-x, y plane and in Fig. 3 on the T-ρ plane.

Barry et al. [16] in 1982 measured 39 points for the excess enthalpy in the vapor phase at three temperatures of 293, 305, and 313 K and at three pressures of 0.5, 1.0, and 1.5 MPa. No other data for the derived thermodynamic properties are available.

5. CORRELATIONS

Helmholtz-type equations of state for the pure components can be expressed in the same functional form as that given in Eq. (1). Subscript 1 is assigned to methane and 2 to hydrogen sulfide. We adopted the equation of state for methane by Setzmann and Wagner [17] published in 1991 and that for hydrogen sulfide by ourselves [18] in 2004. The equation of state for methane by Setzmann and Wagner is widely used as the equation of state recommended by the International Union of Pure and Applied Chemistry (IUPAC) [19]. The equation of state for hydrogen sulfide represents experimental thermodynamic property data with high accuracy. Critical parameters for methane are $T_{c,1} = 190.564\,\mathrm{K}$ and $\rho_{c,1} = 10.139128\,\mathrm{mol \cdot dm^{-3}}$ from Ref. 19. The numerical value of $\rho_{c,1}$ in $\mathrm{mol \cdot dm^{-3}}$ for methane is converted in terms of the molar mass of $0.0160428\,\mathrm{kg \cdot mol^{-1}}$ from $162.66\,\mathrm{kg \cdot m^{-3}}$ originally given by Setzmann and Wagner [17]. The critical parameters for hydrogen sulfide are $T_{c,2} = 373.37\,\mathrm{K}$ and $\rho_{c,2} = 10.20\,\mathrm{mol \cdot dm^{-3}}$ [18].

F_{12} in Eq. (4), k_{12} in Eq. (6) and ξ_{12} in Eq. (9) were fitted based on the experimental data of $P\rho Tx$, VLE, and the critical points. In the fitting process, the following experimental data were used as input data:

(1) 1127 points of $P\rho Tx$ data measured by Reamer et al. [3], which cover the temperature range from 278 to 444 K, the pressure range from 1.4 to 69 MPa, and the composition range from 0.1 to 0.9 mole fraction of methane.

(2) 76 points of (T, P, ρ^{L}, ρ^{V}, x, y) VLE data along the three isotherms of 278, 311, and 344 K measured by Reamer et al. [3], which cover the pressure range from 1.2 to 13 MPa.

(3) 12 points of (T, P, x, y) VLE data measured by Kohn and Kurata [4], which cover the temperature range from 189 to 255 K and the pressure range from 1.4 to 4.1 MPa.

(4) 5 critical-point data measured by Reamer et al. [3] at equal intervals from 0.1 to 0.5 mole fraction.

The numerical values of the temperature for all experimental data were converted to ITS-90.

The behavior of the calculated critical curves varies greatly with the values of k_{12}. Fig. 4 shows the variety of calculated critical curves with $k_{12} = 1.00, 0.95, 0.93, 0.90,$ and 0.85 with ξ_{12} and F_{12} fixed at unity. A continuous critical curve appears with $k_{12} = 1.00$. With decreasing k_{12}, the critical curve changes from Type I to Type III through Type II. The parameter ξ_{12} is sensitive to the representation of $P\rho Tx$ data, but it is not effective in changing the critical curve type. Fixing k_{12} and ξ_{12} at various values, a nonlinear fitting process was repeated to correlate F_{12} based on experimental data. Finally k_{12} and ξ_{12} were fixed at 0.90 and 1.00, respectively. F_{12} was correlated with the function given in Eq. (21).

$$F_{12} = n_0 + n_1 \tau\delta \exp(-\delta) + n_2 \tau\delta^2 \exp(-\delta) + n_3 \tau\delta \exp(-\delta^2), \tag{21}$$

where the numerical constants of the coefficient n_0, n_1, n_2, and n_3 are given in Table II.

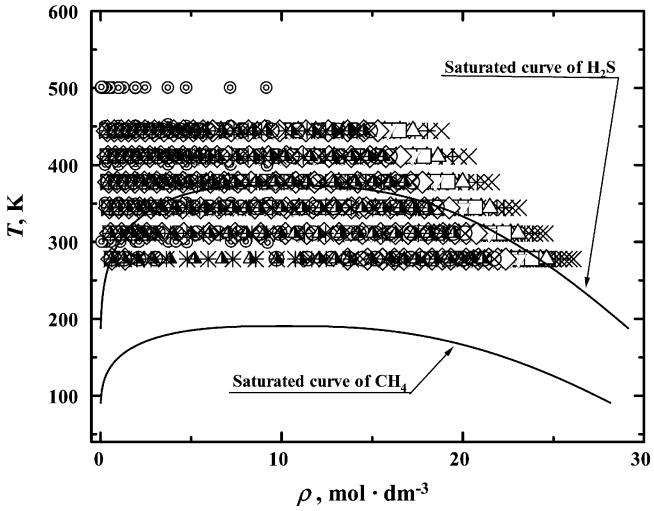

Fig. 1. Distribution of experimental $P\rho Tx$ data. (×) Reamer et al., $x_1 = 0.1$ [3], (+) Reamer et al., $x_1 = 0.2$ [3], (△) Reamer et al., $x_1 = 0.3$ [3], (□) Reamer et al., $x_1 = 0.4$ [3], (▽) Reamer et al., $x_1 = 0.5$ [3], (◇) Reamer et al., $x_1 = 0.6$ [3], (⊗) Reamer et al., $x_1 = 0.7$ [3], (◭) Reamer et al., $x_1 = 0.8$ [3], (✳) Reamer et al., $x_1 = 0.9$ [3], (◎) Bailey et al. $x_1 = 0.5073$ [11].

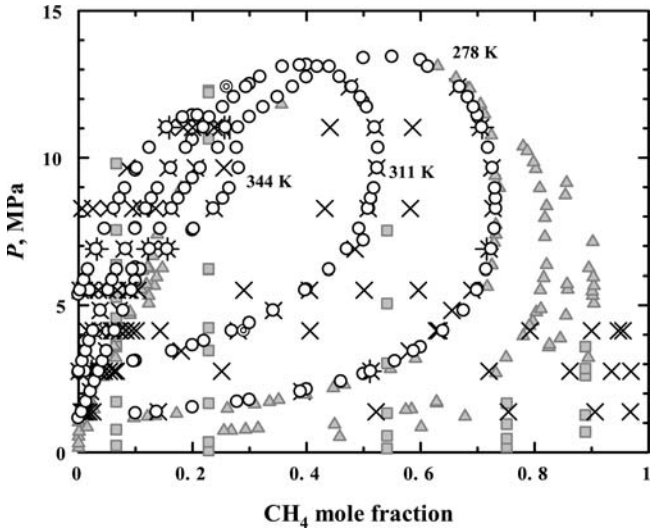

Fig. 2. Distribution of experimental VLE data. (◯) Reamer et al. [3], (◎) Robinson and Bailey [12], (×) Kohn and Kurata [4], (■) Kohn and Kurata [13], (+) Robinson et al. [14], (▲) Yarym-Agaev et al. [15].

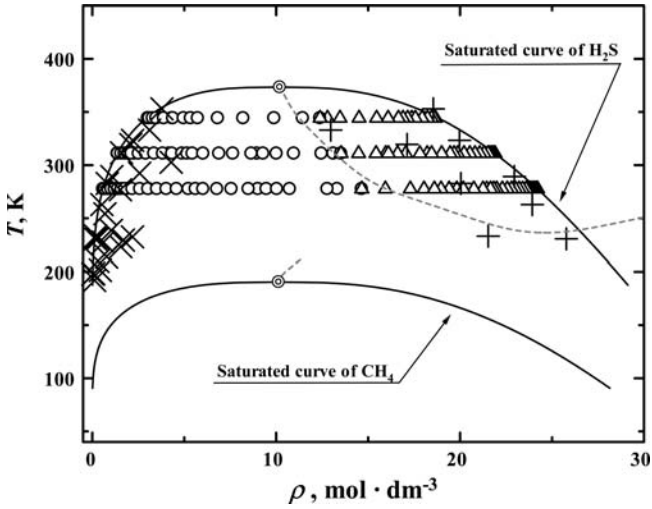

Fig. 3. Distribution of experimental saturated density data. (◯) Reamer et al., ρ^{V} [3], (△) Reamer et al., ρ^{L} [3], (×) Kohn and Kurata, ρ^{V} [13], (+) Kohn and Kurata, ρ^{L} [13], (◎) Critical point of pure component, (– – – – –) Critical curve from the model.

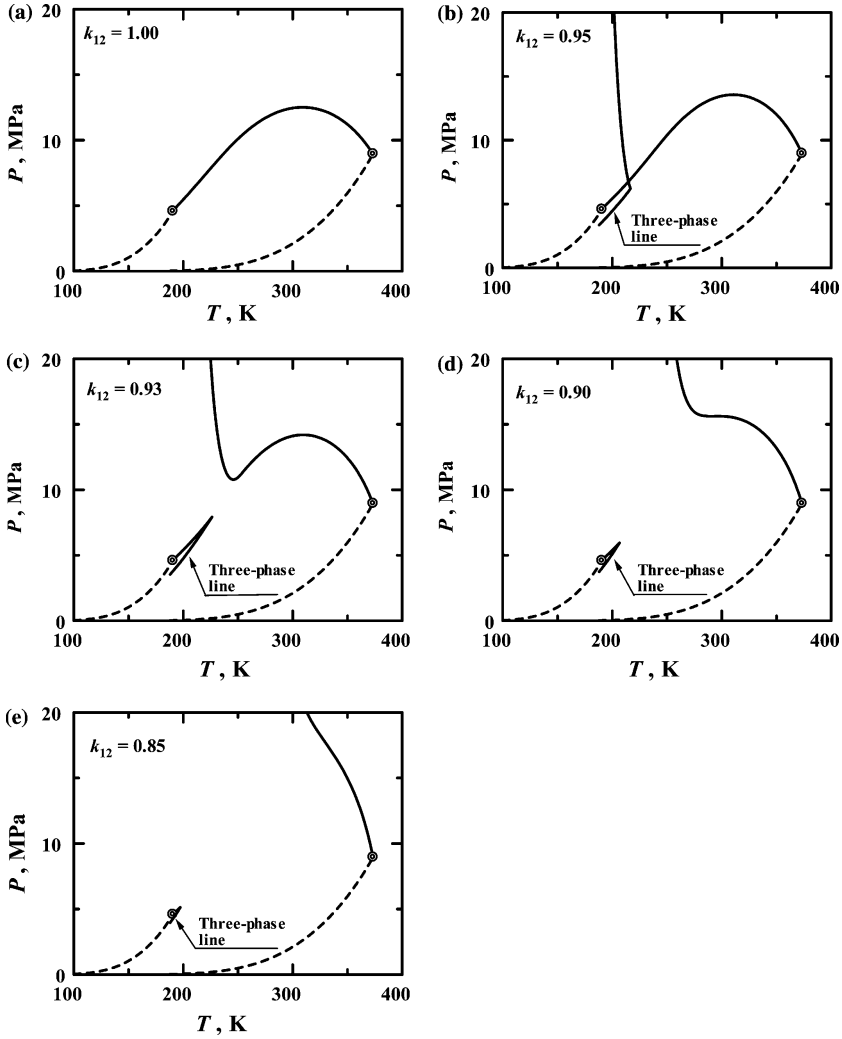

Fig. 4. Behavior of the calculated critical curves for the variety of k_{12} with fixed values of $\xi_{12} = 1.0$ and $F_{12} = 1.0$. (a) $k_{12} = 1.00$, (b) $k_{12} = 0.95$, (c) $k_{12} = 0.93$, (d) $k_{12} = 0.90$, (e) $k_{12} = 0.85$.

6. COMPARISIONS WITH EXPERIMENTAL DATA

6.1. $P\rho Tx$ Property Comparisons

The density deviations of $P\rho Tx$ data from the model are shown in Fig. 5 as a function of pressure and in Fig. 6 as a function of temperature. Reamer et al. [3] measured $P\rho Tx$ data at nine compositions from

Table II. Coefficients of the Model

Parameters	Values
$T_{c,1}$	190.564
$T_{c,2}$	373.37
$\rho_{c,1}$	10.139128
$\rho_{c,2}$	10.20
k_{12}	0.90
ξ_{12}	1.00
n_0	0.90
n_1	0.5517080×10^{0}
n_2	-0.3707104×10^{-1}
n_3	-0.4297850×10^{-1}

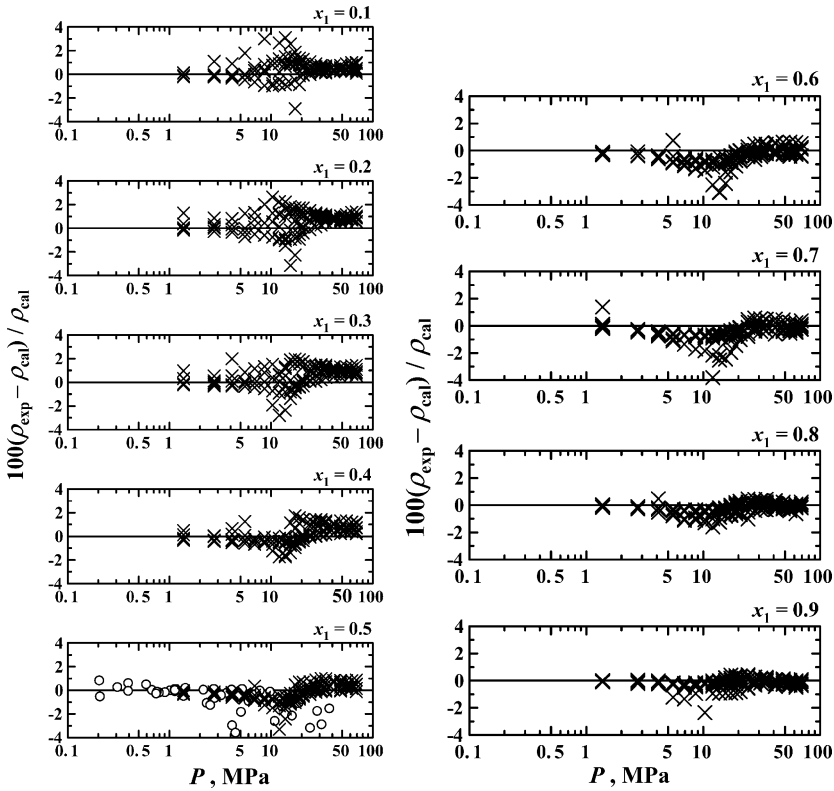

Fig. 5. Density deviations of $P\rho Tx$ data from the model as a function of pressure for different compositions. (×) Reamer et al. [3], (◯) Bailey et al. [11].

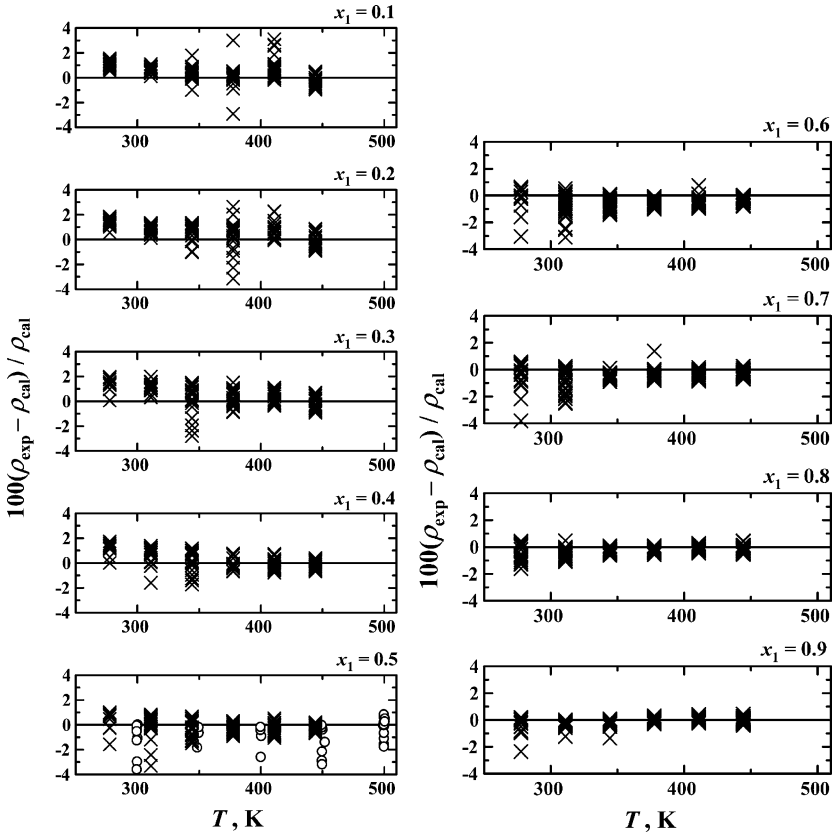

Fig. 6. Density deviations of $P\rho Tx$ data from the model as a function of temperature for different compositions. (×) Reamer et al. [3], (◯) Bailey et al. [11].

0.1 to 0.9 mole fraction of methane in the temperature range from 278 to 444 K and at pressures from 1.4 to 69 MPa. The model represents most of the $P\rho Tx$ data of Reamer et al. within ±2.0% with a bias of 0.01%. The deviations in the high-pressure region (more than 40 MPa) and the low-temperature region (less than 311 K) are systematically larger by about 1% at the compositions from 0.2 to 0.4 mole fraction of methane. Bailey et al. [11] measured $P\rho Tx$ data at 0.5073 mole fraction of methane in the temperature range from 299 to 501 K at pressures up to 38 MPa. Six of their data points in the pressure range from 6 to 13 MPa at 300 K are estimated to be in the two-phase region. The different trends in the $P\rho Tx$ data of Reamer et al. and Bailey et al. are observed in the region of more than 5 MPa and 4.0 $\text{mol} \cdot \text{dm}^{-3}$. The maximum deviation of the $P\rho Tx$

Table III. Statistical Comparisons of the Model with $P\rho Tx$, Saturated Density, and Critical-Point Data

Author[a]	Property	Year	No. of Data	BIAS%	AAD%	SDV%	RMS%	MAX%
Reamer et al.* [3]	$P\rho Tx$	1951	1127	0.01	0.60	0.87	0.87	9.73
Bailey et al. [11]	$P\rho Tx$	1987	65	−1.45	1.53	2.41	2.80	−10.7
Reamer et al. [3]	VLE, ρ^{V}	1951	76	0.91	2.62	3.55	3.64	−12.8
Reamer et al. [3]	VLE, ρ^{L}	1951	76	0.38	1.11	2.20	2.22	10.7
Kohn and Kurata [13]	VLE, ρ^{V}	1959	26	5.49	7.98	10.8	11.9	36.0
Kohn and Kurata [13]	VLE, ρ^{L}	1959	9	4.59	8.10	12.5	12.6	30.9
Reamer et al.* [3]	P_c	1951	9	1.55	1.62	1.42	2.04	2.98
Kohn and Kurata [4]	P_c	1958	2	5.00	5.00	0.87	5.04	5.61
Yarym-Agaev et al. [15]	P_c	1991	7	1.13	1.16	1.57	1.76	3.37
Reamer et al.* [3]	T_c	1951	9	−0.86	1.00	0.94	1.22	−1.90
Kohn and Kurata [4]	T_c	1958	2	−1.10	1.10	1.33	1.44	−2.03
Yarym-Agaev et al. [15]	T_c	1991	7	−0.82	0.98	0.94	1.15	−1.96
Barry et al. [16]	h^{E}	1982	39	−0.77	12.7	16.1	15.9	39.9

[a] Data used as input data are denoted by *.

data of Bailey et al. [11] from the model reaches −11% (excluding the six points). Statistical comparisons of the model with $P\rho Tx$ data are given in Table III.

6.2. VLE and VLLE Property Comparisons

Figure 7 shows composition deviations of VLE data from the model at the bubble point. The upper figure is shown as a function of pressure, and the lower figure is shown as a function of temperature. At the bubble points, the model represents the VLE data of Reamer et al. [3] for the isotherms of 278, 311, and 344 K within ±0.02 mole fraction except near the critical points. Near the critical point, slight pressure differences have large effects on the composition. The model represents the VLE data of Kohn and Kurata [4] within ±0.02 mole fraction in the temperature range from 189 to 366 K except for a few points at 11 MPa. The model shows good agreement with other experimental VLE data for bubble points within ±0.02 mole fraction at pressures up to 10 MPa. At pressures more than 10 MPa, the available VLE data are those near the critical points and their deviations are therefore larger. Most of these VLE data are represented within ±0.04 mole fraction.

Figure 8 shows the composition deviations of VLE data from the model at the dew points. The upper and lower figures are shown as a function of pressure and temperature. At the dew points, the model represents

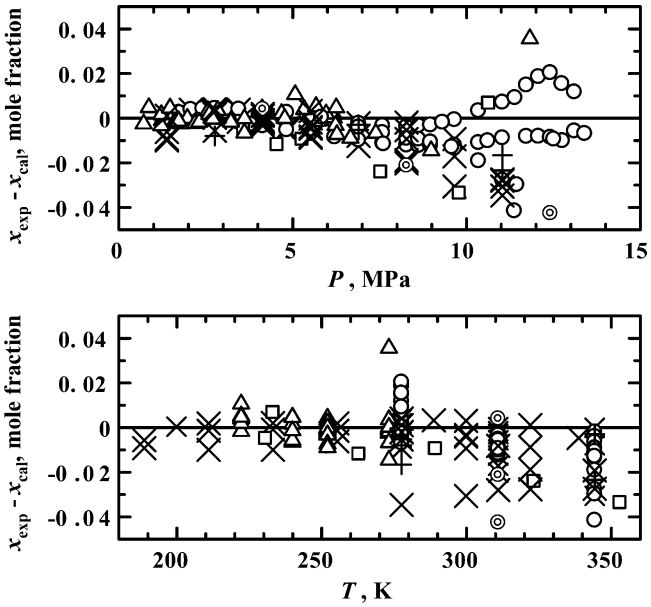

Fig. 7. Composition deviations of VLE data from the model at the bubble point. (◯) Reamer et al. [3], (◎) Robinson and Bailey [12], (×) Kohn and Kurata [4], (□) Kohn and Kurata [13], (+) Robinson et al. [14], (△) Yarym-Agaev et al. [15].

most of the VLE data of Reamer et al. [3] and those of Kohn and Kurata [4] within ±0.03 mole fraction. At low pressures, comparatively large deviations are shown because slight differences in pressure again have large effects on the composition. The deviations of most of the VLE data of Yarym-Agaev et al. [15] from the model are within ±0.04 mole fraction. The deviations of the VLE data of Kohn and Kurata [13] are within ±0.15 mole fraction at the dew points.

Four phase-equilibrium isotherms at 189, 278, 311, and 344 K calculated from the model are shown in Fig. 9 along with experimental VLE data. The calculated isotherms are in good agreement with these experimental data. At 278, 311, and 344 K, the calculated phase-equilibrium isotherms describe common VLE curves similar to Type I. However, VLLE appears at 189 K. The pressure of the VLLE point at 189 K calculated from the model is 3.712 MPa. The compositions of the three coexisting phases are 0.097, 0.897, and 0.982 mole fraction of methane and the densities are 28.10, 18.07, and 4.04 $mol \cdot dm^{-3}$, respectively. For the 189 K isotherm, the VLE is shown in the low-pressure region below the pressure of the VLLE state. LLE appears above the pressure of the VLLE

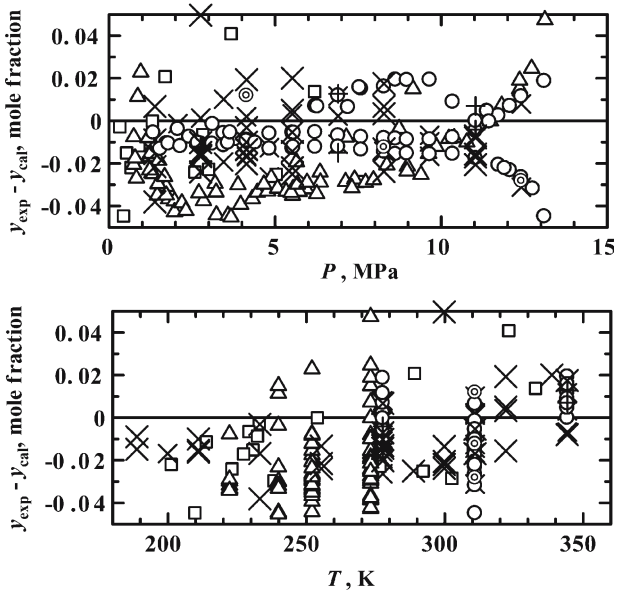

Fig. 8. Composition deviations of VLE data from the model at the dew point. (◯) Reamer et al. [3], (◎) Robinson and Bailey [12], (×) Kohn and Kurata [4], (□) Kohn and Kurata [13], (+) Robinson et al. [14], (△) Yarym-Agaev et al. [15].

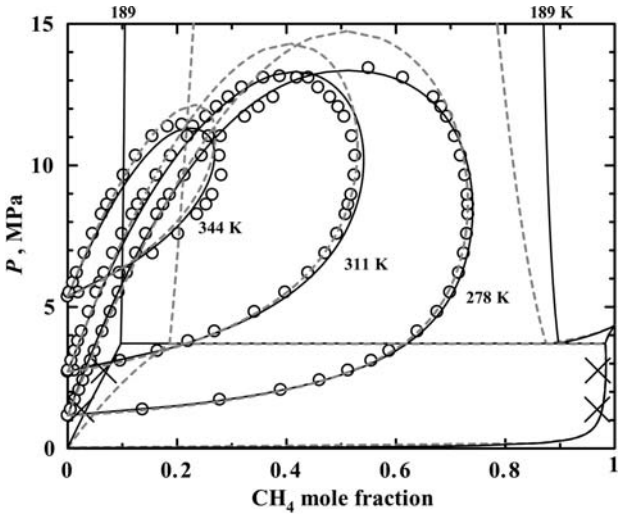

Fig. 9. Behavior of the phase equilibrium calculated from the model and the PR-type equation of state. (◯) Reamer et al. [3], (×) Kohn and Kurata [4], (– – – –) Endo et al. [5], (——) Model.

state. The model at 189 K is in good agreement with the VLE data of Kohn and Kurata [4] although they did not report numerical information about VLLE and LLE. Statistical comparisons of the model with experimental VLE composition data are shown in Table IV for bubble and dew points.

6.3. ρ^{L} and ρ^{V} Comparisons

Figure 10 shows the behavior of saturated densities calculated from the model with the critical curve (which is also calculated from the model), along with experimental data on the $\rho - x$ plane. In this figure, the three isotherms 278, 311, and 344 K are also plotted. The model shows good agreement with these experimental data. The density deviations of the VLE data of Reamer et al. [3] from the model are within 3% at the bubble points and within 7% at the dew points except near the critical region. The density deviations of most of the VLE data of Kohn and Kurata [13] from the model are within 5% at the bubble points and within 8% at the dew points. The statistical comparisons of the model are shown in Table III.

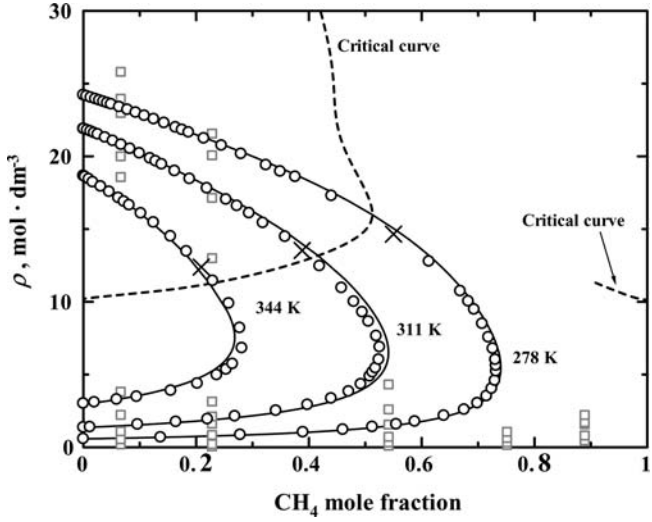

Fig. 10. Saturated densities along the 278, 311, and 344 K isotherms and critical curves calculated from the model. (◯) Reamer et al. [3], (□) Kohn and Kurata [13], (×) Critical point of Reamer et al. [3], (———) Saturation curve calculated from the model, (– – – –) Critical curve calculated from the model.

Table IV. Statistical Comparisons of the Model and the PR-type Equation of State with VLE Composition Data

Author[a]	Property	Year	No. of Data	The Model					The PR-type EOS				
				BIAS	AAD	SDV	RMS	MAX	BIAS	AAD	SDV	RMS	MAX
Reamer et al.* [3]	VLE, y	1951	76	−0.005	0.012	0.015	0.016	0.059	−0.008	0.015	0.022	0.023	−0.098
Reamer et al.* [3]	VLE, x	1951	76	−0.003	0.007	0.009	0.009	−0.028	0.012	0.015	0.028	0.030	0.140
Robinson and Bailey [12]	VLE, y	1957	3	−0.009	0.017	0.020	0.019	−0.028	−0.007	0.018	0.027	0.023	−0.037
Robinson and Bailey [12]	VLE, x	1957	3	−0.020	0.023	0.023	0.028	−0.043	−0.002	0.008	0.011	0.009	−0.014
Kohn and Kurata* [4]	VLE, y	1958	61	−0.008	0.014	0.015	0.016	0.050	−0.005	0.012	0.015	0.015	0.042
Kohn and Kurata* [4]	VLE, x	1958	59	−0.008	0.009	0.011	0.014	−0.035	−0.009	0.010	0.013	0.016	−0.066
Kohn and Kurata [13]	VLE, y	1959	26	0.006	0.037	0.050	0.049	0.149	−0.000	0.034	0.045	0.044	0.133
Kohn and Kurata [13]	VLE, x	1959	9	−0.023	0.024	0.022	0.031	−0.054	−0.024	0.026	0.027	0.035	−0.091
Robinson et al. [14]	VLE, y	1959	5	−0.002	0.010	0.012	0.011	−0.015	−0.002	0.009	0.011	0.010	0.018
Robinson et al. [14]	VLE, x	1959	5	−0.011	0.011	0.009	0.014	−0.023	−0.003	0.005	0.007	0.007	−0.011
Yarym-Agaev et al. [15]	VLE, y	1991	78	−0.020	0.027	0.023	0.031	0.105	−0.025	0.028	0.018	0.031	0.090
Yarym-Agaev et al. [15]	VLE, x	1991	46	0.000	0.004	0.007	0.007	0.036	−0.011	0.014	0.018	0.021	0.062

[a] Data used as input data are denoted by *.

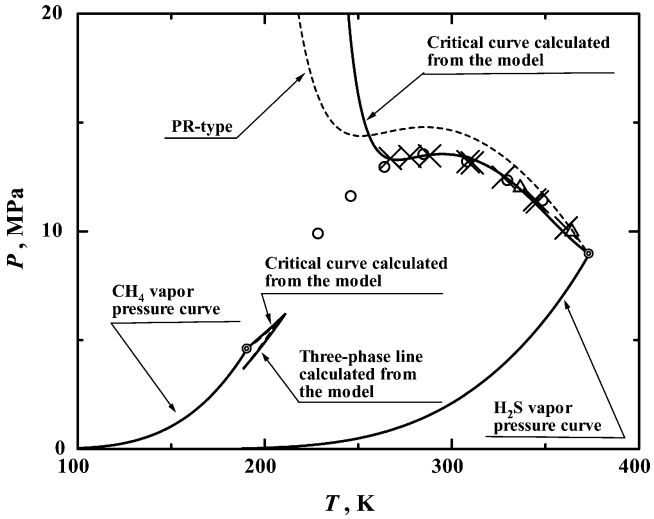

Fig. 11. Critical curves calculated from the model and the PR-type equation of state with the experimental data. (×) Reamer et al. [3], (△) Kohn and Kurata [4], (◯) Yarym-Agaev et al. [15], (◎) Critical point of pure component, (– – – –) Endo et al. [5], (———) Model.

6.4. Critical Curve Comparisons

Figure 11 shows the behavior of the critical curves calculated from the model. The model shows divergence of the critical curve starting from the critical point of hydrogen sulfide to the high-pressure region. The critical curve that starts from the critical point of methane is terminated at the intersection with the three-phase line of VLLE. The intersection is called the "Upper Critical End Point" and its composition is 0.909, temperature is 210.919 K, pressure is 6.195 MPa, and density is $11.30\,\mathrm{mol}\cdot\mathrm{dm}^{-3}$ calculated from the model. It is estimated that the binary mixture of methane and hydrogen sulfide does not have critical points between 0.513 and 0.909 mole fraction of methane. The model is in good agreement with the critical-point data of Reamer et al. [3] within ±3% for pressure calculations and ±2% for temperature calculations. The temperature deviations of the critical-point data of Kohn and Kurata [4] from the model are within ±2% although the maximum pressure deviation reaches 5.6%. The deviations of the critical-point data of Yarym-Agaev et al. [15] from the model are within ±3.4% for pressure calculations and ±2% for temperature calculations in the composition range from 0.2 to 0.5 mole fraction of methane, but they show that the critical curve of the binary mixture of

methane and hydrogen sulfide is a continuous line. Statistical comparisons of the model with the critical pressures and temperatures are shown in Table III. Reamer et al. [3] reported three critical density points at 0.209, 0.388, and 0.550 mole fraction of methane. The critical point at 0.550 mole fraction of methane was not observed by Kohn and Kurata [13]. The density deviations of the critical density data by Reamer et al. from the model are 11.1% at 0.209 mole fraction and 5.7% at 0.388 mole fraction of methane.

6.5. Molar Excess Enthalpy Comparisons

Figure 12 shows the behavior of the molar excess enthalpy calculated from the model with the experimental data of Barry et al. [16]. They measured molar excess enthalpies in the gas phase for three temperatures of 293, 305, and 313 K at three pressures of 0.5, 1.0, and 1.5 MPa. Statistical comparisons of the model with these data are shown in Table III.

7. COMPARISIONS WITH THE PR-TYPE EQUATION OF STATE

Cubic equations of state can represent complicated phase equilibrium and the critical curve with a few parameters. We made comparisons with the PR-type equation of state developed by Endo et al. [5]. Figure 9 shows the phase equilibrium behavior of the PR-type equation of state and our model. In the temperature region above 278 K, both equations of state show good agreement with the VLE data of Reamer et al. [3], although the PR-type equation of state does not represent the VLE data of Reamer et al. accurately enough near the critical region. At 189 K, the PR-type equation of state shows good agreement with the model and the experimental data in the methane rich side of the VLE region below the VLLE pressure as shown in Fig. 9. In the hydrogen sulfide rich side of the VLE at 189 K, the bubble-point curve calculated from the PR-type equation of state shows much larger mole fractions of methane than that from our model and shows large differences from the experimental data of Kohn and Kurata [4], whereas our model shows good agreement with these experimental data. For VLLE at 189 K, we calculated from the PR-type equation of state the pressure of the three-phase line to be 3.698 MPa, the three coexisting compositions to be 0.186, 0.875, and 0.983, and the densities at these compositions to be 30.47, 20.08, and 4.15 $\text{mol} \cdot \text{dm}^{-3}$. The pressure of VLLE at 189 K calculated from our model is 3.712 MPa, which is 0.4% larger than the value of the PR-type equation of state.

Statistical comparisons of our model and the PR-type equation of state with experimental VLE composition data are shown in Table IV. The values listed in Table IV are expressed using the difference between

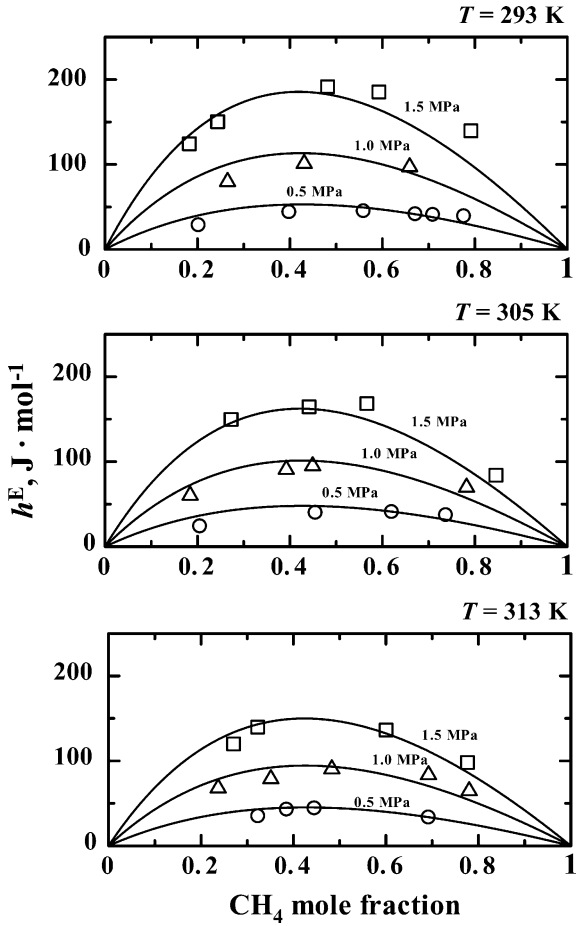

Fig. 12. Behavior of molar excess enthalpy calculated from the model with the experimental data. (◯) Barry et al., $P =$ 0.5 MPa [16], (△) Barry et al., $P = 1.0$ MPa [16], (□) Barry et al., $P = 1.5$ MPa [16].

the experimental mole fraction and that calculated from our model. Our model shows good agreement with the experimental data. The agreement of the PR-type equation of state with the experimental data is as good as our model. However, our model agrees better with the experimental data near the critical points.

Cubic equations of state such as the PR-type equations of state are not as good in representing the density. Figure 13 shows the behavior of saturated densities along the 250, 300, and 350 K isotherms from the

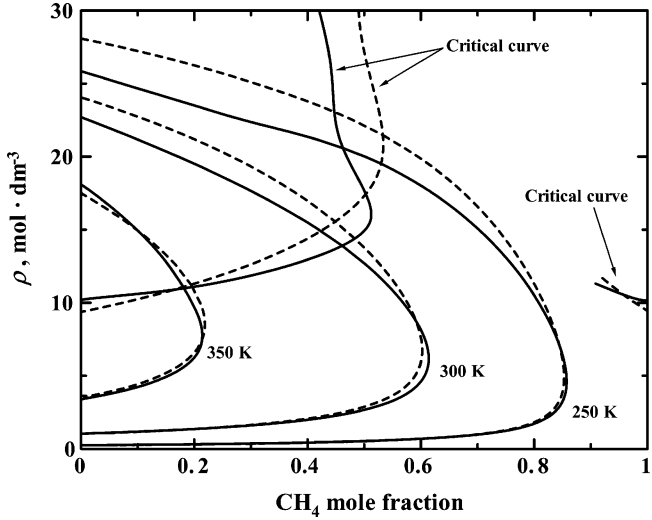

Fig. 13. Comparison of saturated densities along the 250, 300, and 350 K isotherms and critical curves calculated from the model and PR-type equation of state. (– – – –) Endo et al. [5], (———) Model.

model and the PR-type equation of state along with the critical curves. The PR-type equation of state is in good agreement with the model in the vapor phase. However, in the liquid phase the PR-type equation of state is different from the model, particularly in the high-density region such as that at 250 K. As shown in Fig. 11, the critical curve of the PR-type equation of state shows divergence, but it does not represent the experimental data as well as our model.

8. UNCERTAINTY ESTIMATION

Based on the results of comparisons between the model and experimental data, the uncertainty in density calculations is estimated to be 2%. The uncertainty in vapor-liquid equilibrium calculations is 0.02 mole fraction in liquid phase and 0.03 mole fraction in vapor phase. The model also represents the critical points with an uncertainty of 2% in temperature calculations and 3% in pressure calculations.

REFERENCES

1. R. L. Scott and P. H. van Konynenburg, *Discuss. Faraday Soc.* **49**:87 (1970).
2. J. S. Rowlinson and F. L. Swinton, *Liquids and Liquid Mixtures* (Butterworth Scientific, London, 1982), pp. 191–194.

3. H. H. Reamer, B. H. Sage, and W. N. Lacy, *Ind. Eng. Chem.* **43**:976 (1951).
4. J. P. Kohn and F. Kurata, *AIChE J.* **4**:211 (1958).
5. T. Endo, D. Arai, and M. Uematsu, *Nippon Kikai Gakkai Ronbunshu, B-hen.* **59**:529 (1993).
6. E. W. Lemmon and R. T. Jacobsen, *Int. J. Thermophy.* **20**:825 (1999).
7. P. J. Mohr and B. N. Taylor, *J. Phys. Chem. Ref. Data*, **28**:1713 (1999).
8. M. L. Michelsen, *Fluid Phase Equilib.* **9**:1 (1982).
9. T. Nitta, K. Ikeda, and T. Katayama, *Fluid Phase Equilib.* **53**:105 (1989).
10. R. A. Heidemann and A. M. Khalil, *AIChE J.* **26**:769 (1980).
11. D. M. Bailey, C. H. Liu, J. C. Holste, K. R. Hall, P. T. Eubank, and K. N. Marsh, *GPA Research Report 107*, Gas Processors Assoc., Tulsa, Oklahoma (1987).
12. D. B. Robinson and J. A. Bailey, *Can. J. Chem. Eng.* **35**:151 (1957).
13. J. P. Kohn and F. Kurata, *J. Chem. Eng. Data* **4**:33 (1959).
14. D. B. Robinson, A. P. Lorenzo, and C. A. Macrygeorgos, *Can. J. Chem. Eng.* **37**:212 (1959).
15. N. L. Yarym-Agaev, L. D. Afanasenko, V. G. Matvienko, Y. Y. Ryabkin, and G. B. Tolmacheya, *Ukrainskii Khimicheskii Zhurnal* (Russ. Ed.) **57**:701 (1991).
16. A. O. Barry, S. C. Kaliaguine, and R. S. Ramalho, *J. Chem. Eng. Data* **27**:436 (1982).
17. U. Setzmann and W. Wagner, *J. Phys. Chem. Ref. Data* **20**:1061 (1991).
18. N. Sakoda and M. Uematsu, *Int. J. Thermophys.* **25**:709 (2004).
19. W. Wagner and K. M. de Reuck, *Methane, International Thermodynamic Tables of the Fluid State*, Vol. 13 (Blackwell Science, 1996).